

Well ties for seismic with severe stratigraphic filtering

Chen Qi¹ and Fred Hilterman²

ABSTRACT

Stratigraphic filtering (SF), or short-period multiples, is prominent in cyclically stratified sedimentation with large impedance contrasts that result in normal-incident reflection magnitudes greater than 0.5. Because SF attenuates and delays the propagating wavelet, similar to the effects of Q attenuation, the integrity of well ties is often jeopardized. A method is proposed to obtain better well ties in areas with severe SF. Starting with a well-log acoustic impedance curve, two-way transmitted wavefields and their equivalent inverse filters are generated at each time sample. Because a time-varying convolution of the transmitted wavefields with the primary-only reflectivity yields the multiple reflectivity, a time-varying deconvolution of the multiple synthetic with the inverse filters yields the primary-only reflectivity. In essence, when the multiple synthetic matches the near-angle stack at a well location, the near-angle stack is deconvolved in a time-varying fashion to match the primary-only synthetic, which then constitutes a correlation with the acoustic impedance yielding a good well tie. This new well-tie technique preserves the integrity of the lithologic interpretation because stretching and squeezing the time scale of the primary-only synthetic to force a seismic match are avoided. Our well-tie method is applied to the synthetic and field data from Cooper Basin, Australia, where more than 30 coal beds are observed within a 1000 ft (304 m) interval.

INTRODUCTION

In reflection seismology, one of the main processing objectives is to image reflections from geologic boundaries. However, because of the earth's structural complexities and various propagation effects, the fidelity of the processed image often requires validation such as

a well tie. This seismic correlation to the well-log formation tops is normally accomplished with a primary-only synthetic seismogram. However, interpreters often stretch and/or squeeze the synthetic time scale to facilitate a reasonable seismic correlation to account for velocity dispersion associated with attenuation and short-period multiples. An apparent attenuation arises when a propagating wavelet traverses numerous thin beds with large impedance contrasts yielding what is called stratigraphic filtering (SF). This attenuation is often larger than the intrinsic attenuation through the same travel path (Margrave, 2015). The main effects of SF on the propagating wavelet were analyzed in a classic paper by O'Doherty and Anstey (1971).

"Short period" indicates that the time difference between the primary reflection and the first-order multiple reflection is less than the period of the propagating wavelet (Banik et al., 1985b). As O'Doherty and Anstey demonstrate, SF delays, shapes, and magnifies the transmitted pulse (compared with the primary transmission loss), and the spectrum of the transmitted pulse is closely related to the spectrum of the primary reflection coefficients. The relationship between the reflection and transmission spectra has been widely studied since it was first proposed by O'Doherty and Anstey (1971). The original formula only deals with amplitude spectra and was extended to the phase spectra by Banik et al. (1985a) who derive the O'Doherty and Anstey formula in continuum media using the 1D stochastic wave equation and the mean field theory. They also point out the scale-dependent attenuation effect of SF. In depositional sequences composed of two different lithologies that are cyclical, not only the magnitude of reflection coefficients but also the ratios of the periodicity affect SF (Stovas et al., 2007). In the low-frequency band, the layered structure behaves as an effective medium with an effective group velocity that introduces reflection time delays.

There are numerous techniques to remove attenuation effects from seismic data, including processes in the time-frequency domain and nonstationary deconvolution (such as Gabor deconvolution and inverse Q -filters). Mathieu (2013) combines the autoregressive signal estimation and Q -compensation to improve the temporal resolution. However, there are few published techniques

Manuscript received by the Editor 20 December 2016; revised manuscript received 5 March 2017; published ahead of production 12 May 2017; published online 21 June 2017.

¹University of Houston, Houston, Texas, USA. E-mail: geophysics.chen.qi@gmail.com.

²Geokinetics Inc., Houston, Texas, USA. E-mail: fred.hilterman@geokinetics.com.

© 2017 Society of Exploration Geophysicists. All rights reserved.

that successfully remove the effects of SF short-period multiples. Margrave et al. (2011) propose a nonstationary Gabor deconvolution method to remove time-varying attenuation effects. However, as the authors state, the nonstationary convolution model (equation 7 in Margrave et al., 2011) that includes the source wavelet and attenuation excludes the “very short-period reverberations leading to the effective Q of O’Doherty and Anstey (1971).”

In this paper, we show that a rejection of high-frequency components in the seismic increases the seismic-to-borehole correlation significantly when strong SF effects exist. In addition, we offer an interpretation technique that correlates multiple synthetics to primary-only synthetics when severe SF exists.

SF AND THE WELL TIE

Severe SF typically occurs in coal-bed regions. Qi and Hilterman (2014) analyze the well-tie problem due to coal beds for Cooper Basin, Australia. In Figure 1, a synthetic with primary-only reflections along with a synthetic with interbed multiples shows different levels of correlation to the adjacent seismic near-offset stack. The Waters (1987) algorithm was used to generate the 1D synthetic seismogram with all orders of multiples except surface multiples. Both synthetic seismograms have been shifted to tie with the top of the coal beds at 1850 ms. Obviously, the synthetic seismogram with multiples (Figure 1a) correlates better to the near-offset stack than does the primary-only synthetic (Figure 1c). However, the multiple synthetic does not directly relate to the impedance log shown in Figure 1b, and this makes the lithologic interpretation difficult.

As will be shown in the next section, it is difficult to remove severe short-period interbed multiples due to the combined effects of signal attenuation and noise coda generated by the SF process (Qi and Hilterman, 2015). However, we found an efficient interpretation process using progressive deconvolution to tie a multiple synthetic

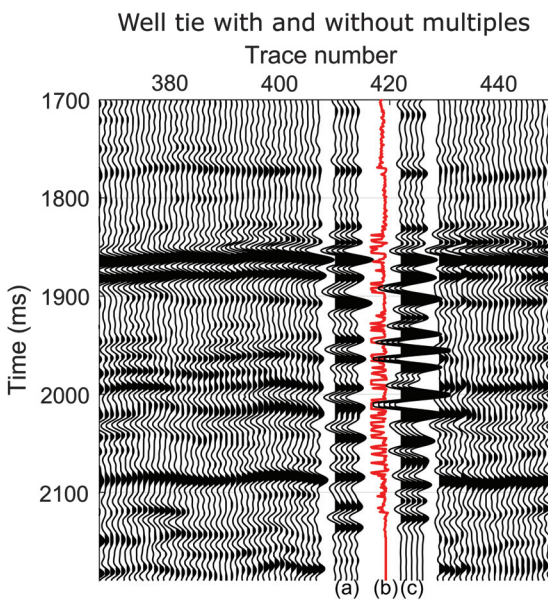


Figure 1. Near-offset seismic data with (c) primary-only synthetic and (a) primary plus multiple synthetic. (b) Both synthetic seismograms are generated from the same impedance log. The initial propagating wavelet was extracted at the top of the coal beds (1850 ms).

to a primary-only synthetic such that a correlation between the seismic and the impedance log can be built.

PRIMARY, GENERALIZED PRIMARY, AND TWO-WAY TRANSMITTED WAVEFIELD

In our synthetic models, the earth is assumed to be elastic and horizontally stratified with vertically traveling plane P-waves (Robinson, 1968). The two-way traveltime in each layer is equal to one

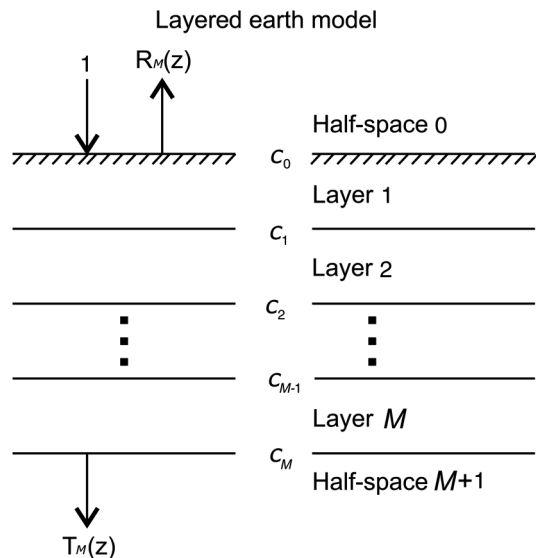


Figure 2. Notation for the layered earth model.

Raypaths of two-way transmitted wavefield

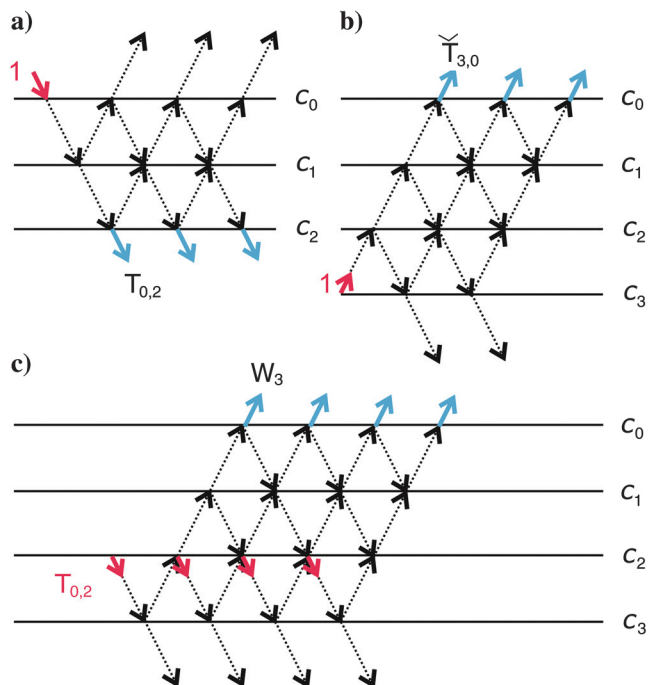


Figure 3. Raypaths corresponding to the two-way transmitted wavefield reflected at interface 3.

time unit. The mathematical notation used by Goupillaud (1961), Kunetz (1964), Treitel and Robinson (1966), and Claerbout (1968) is illustrated in Figure 2. The upper half-space (air) is layer 0, and c_M is the reflection coefficient of the bottom interface of layer M . The impulse response for reflection and transmission is expressed by the z -transforms as

$$R_M(z) = \sum_{n=0}^M R_n z^n \quad (1)$$

$$T_M(z) = \sum_{n=0}^M T_n z^n, \quad (2)$$

where R_n and T_n represent the reflection and transmission responses at time n , respectively.

For analyzing SF effects, a unit-amplitude spike is applied just above the upper interface of layer 1 as shown in Figure 2. Hubral et al. (1980) propose a decomposition method in equation 1 for generating synthetic seismograms with multiples. He introduces “generalized

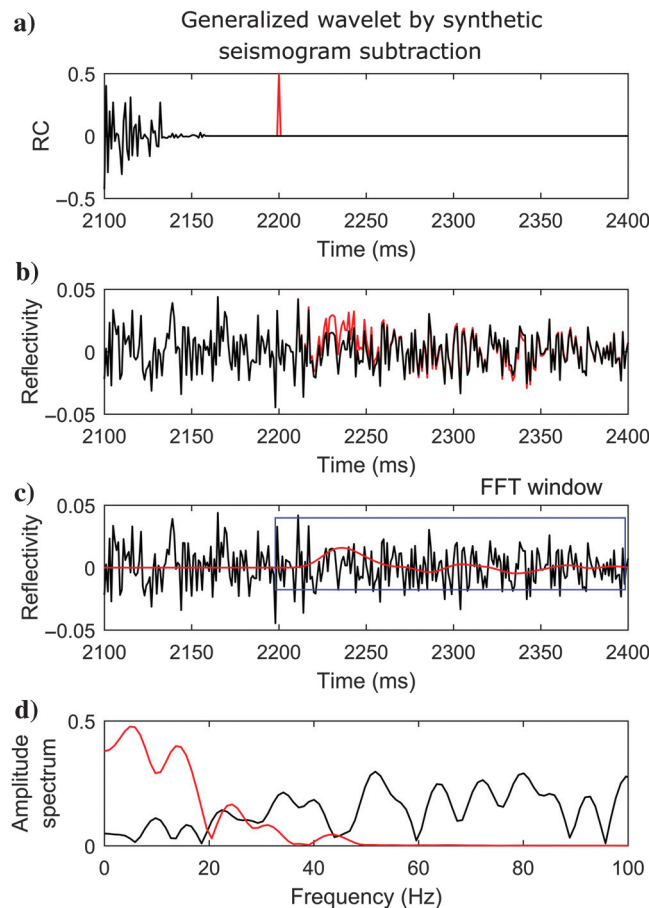


Figure 4. Generalized wavelet by synthetic seismogram subtraction. (a) The black curve is well-log reflectivity, whereas the red curve is the same as the black with an extra reflection coefficient at 2200 ms. (b) Synthetic seismograms from the unit spike are generated with extra reflection (red) and without (black). (c) The difference of two synthetics is the red curve and the black curve is the same as the black curve in (b). (d) Spectra of the red and black curves in (c) are displayed as red and black, respectively.

primaries” such that the superposition of all the generalized primaries (with proper time shifts) exactly equals the synthetic seismogram $R_M(z)$ with all possible raypaths. This process is expressed as

$$R_M(z) = \sum_{i=0}^M W_i(z) z^i, \quad (3)$$

where $W_i(z)$ is the generalized primary reflection for the interface i . Using the fundamental polynomials proposed by Robinson (1967), Hubral et al. (1980) derive the expression for the generalized primary as

$$W_i(z) = \frac{c_i}{1 + c_i} T_{0,i}(z) T_{i-1,0}(z) z^{-i+\frac{1}{2}}, \quad (4)$$

where c_i is the reflection coefficient for interface i and $T_{0,i}(z)$ represents the transmission response for an impulse source impinging just above interface 0 and transmitted through layer 1 to just beneath interface i . Equation 4 can also be expressed as

$$W_i(z) = c_i T_{0,i-1}(z) \hat{T}_{i,0}(z) z^{-i+\frac{1}{2}}, \quad (5)$$

$$\hat{T}_{i,0}(z) = \frac{1}{1 + c_i} T_{i,0}(z). \quad (6)$$

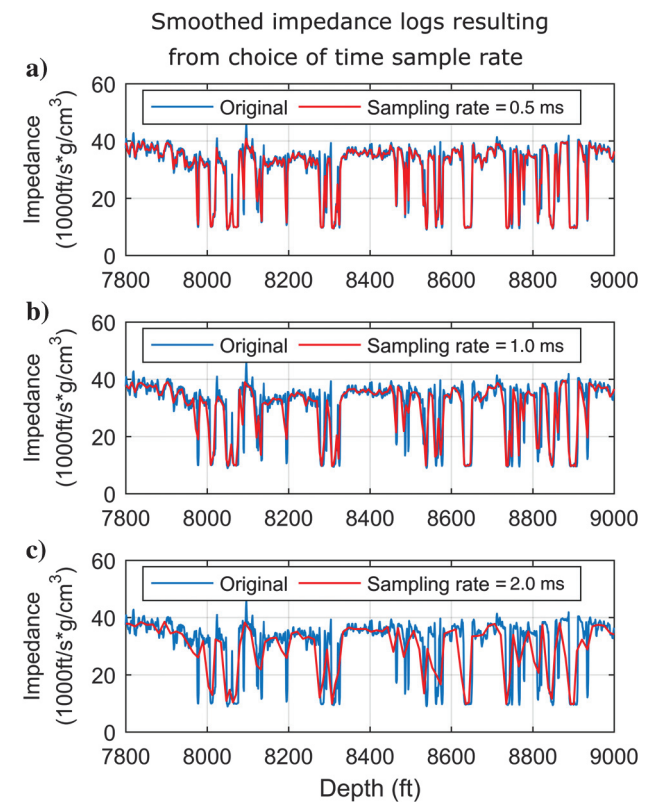


Figure 5. Smoothed impedance logs resulting from the choice of the time sample rate. The depth-domain impedance log was converted to depth using (a) 0.5 ms, (b) 1 ms, and (c) 2 ms sample rates. After converting to time, the logs were reconverted to depth using a time-depth table.

In this way, the generalized primary is expressed as the convolution between two transmission responses due to a downward source at the top interface and the other as an upward source at the bottom layer. The downward $T_{0,i-1}(z)$ traverses the model with all interfaces above interface i , and the upward one $\hat{T}_{i,0}(z)$ traverses the model with all interfaces above and including interface i . Figure 3a–3c illustrates the raypaths for $T_{0,2}(z)$, $\hat{T}_{3,0}(z)$, and $W_3(z)$, respectively. The red arrows represent the upward and downward sources, and the blue arrows represent the model outputs. The convolution of the transmission responses in Figure 3a and 3b describes the following physical process: A downward source in Figure 3a generates a wavefield just beneath interface 2, which is depicted by three blue arrows in Figure 3a. This wavefield becomes the source in Figure 3c depicted by the downward traveling red arrows.

The two-way transmitted wavefield is equivalent to the generalized primary normalized by the corresponding reflection coefficient:

$$\hat{W}_i(z) = \frac{W_i}{c_i}. \quad (7)$$

Stratigraphic effects on synthetic seismograms and transmitted wavelets

- Sampling rate = 0.5 ms
- Sampling rate = 1.0 ms
- Sampling rate = 2.0 ms
- Seismic

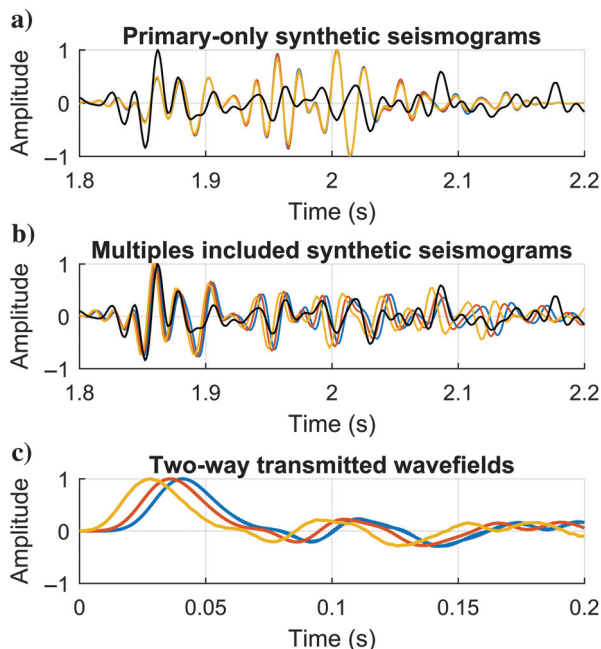


Figure 6. Stratigraphic effects on synthetic seismograms and transmitted wavelets. (a) Primary-only synthetic seismograms generated from time-domain impedance logs with sampling rates of 0.5, 1, and 2 ms, respectively, are plotted against the seismic trace at the well location. Primary-only synthetics overlap each other. (b) The same synthetic seismograms but with multiples included are plotted again to illustrate the impact of different sampling rates. (c) Two-way transmitted wavefields reflected from the bottom of the coal bed sequence (at 9000 ft in Figure 5) are plotted together to illustrate the effects of different sampling rates.

Examples and detailed steps to generate a two-way transmitted wavefield have been documented by Qi (2013) and Qi and Hilterman (2014).

To interpret lithologic events, SF effects should be suppressed. Lupinacci et al. (2017) provide a novel three-stage Q -factor compensation method for poststack seismic data. They incorporate the Q estimation, high-frequency noise removal, and stable inverse Q filtering in the workflow. The promising results shown in their paper indicate a possible solution for SF effects if

- 1) the SF attenuation can be accurately defined and
- 2) high-frequency noise coda can be predicted and removed.

Margrave (2015) analyzes 1D synthetic seismograms with multiples and intrinsic Q attenuation using Ganley's (1981) algorithm. He compares the measured constant- Q value with the provided intrinsic Q value and concludes that the biased Q measurements were due to the effective constant- Q attenuation introduced by SF. However, using two-way transmitted wavelets, we proposed an alternate to the constant- Q attenuation model for SF. Qi and Hilterman (2014) analyze the SF attenuation effects of thin coal beds from Cooper Basin, Australia, that had consistent reflection magnitudes of approximately 0.6. Because of this large reflection magnitude, they propose a Gaussian-attenuation model to account for the signal broadening and time-delay effects due to the SF process. The Gaus-

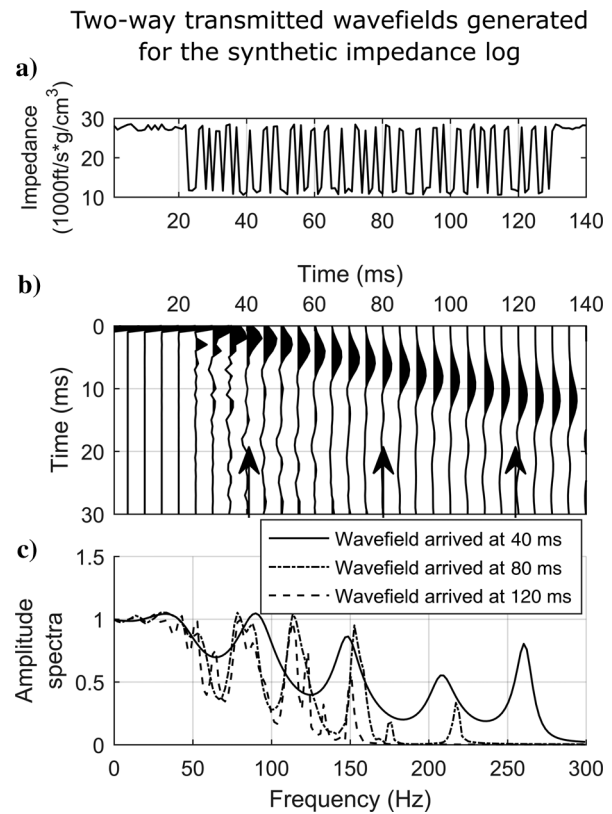


Figure 7. (b) Two-way transmitted wavefields generated from the synthetic impedance log in (a). (c) The spectra for the two-way transmitted wavefields are plotted for the locations at the top, middle, and bottom of the stratigraphic sequence. (a) The impedance log and (b) the two-way transmitted wavefields share the same horizontal axis.

sian-attenuation model is different from the constant- Q attenuation model in terms of the power of the frequency term,

$$A_Q(f, \Delta x) \approx \exp(-\Delta x \alpha f^2), \quad (8)$$

where Δx represents the distance from the top of the coal sequence to the measurement point in the coal sequence, f is the frequency, α is a parameter related to the standard deviation of the Gaussian wavelet in the time domain, and A_Q is the amplitude spectrum of the signal. The main difference between the Gaussian-attenuation model and the constant- Q attenuation model is that the constant- Q attenuation model is a function of frequency to the first power (approximately) and the Gaussian-attenuation model to the second power. With the proposed attenuation equation, inverse Q -filtering or other time-varying deconvolution methods such as Gabor deconvolution (Margrave et al., 2011) will attempt to compensate for the broadening of the signal portion of the generalized wavelet but will also enhance the high-frequency noise.

A simple numeric model illustrates the signal and noise from SF. In Figure 4a, a reflection coefficient of 0.5 is placed at 2200 ms, which is 100 ms past the end of the well-log curves. Using a spike source, synthetic seismograms with multiples are generated with and without the extra reflector (red and black, respectively, in Figure 4b). A subtraction of the two synthetic seismograms generates the two-way transmitted wavefield, which is the red curve in Figure 4c. The black curve in Figure 4c represents the synthetic seismogram without the extra reflector, and all the energy after 2130 ms is noise coda. The amplitude spectrum of the signal (Figure 4d; red) lies in the low-frequency range from 0 to 20 Hz, whereas the am-

Synthetic seismograms with and without interbed multiples

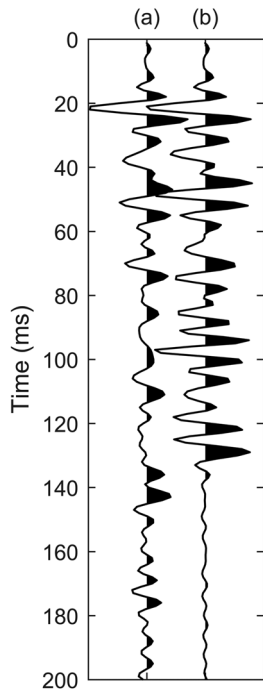


Figure 8. (a) Synthetic seismogram with multiple and primary reflections and (b) synthetic with primary-only reflections generated using the impedance model shown in Figure 7a.

plitude spectrum of the noise from 2200 to 2400 ms (Figure 4d; black) concentrates in the high-frequency range of greater than 20 Hz. A deconvolution of the red curve in Figure 4b would enhance the noise coda more than it enhances the signal in the frequency range greater than 20 Hz. Trying to flatten the red signal spectrum greater than 20 Hz in Figure 4d will undesirably increase the black noise spectrum. An alternative way to compensate for the SF attenuation is to apply a time-varying high-cut filter to remove the noise and then increase the signal portion with spectral broadening in the time-frequency domain.

SF AND DEPTH-TO-TIME SAMPLE RATE

Before calculating synthetic seismograms and two-way transmitted wavefields using equation 7, the original depth-domain impedance log needs to be converted to the time domain. The seismic data shown in Figure 1 were sampled at 2 ms. However, if the impedance log, which is sampled at a 1 ft interval, is transformed to time at a 2 ms interval (Figure 5c), the character of the impedance log in time is smoothed, which will decrease the effects of SF (Banik et al.,

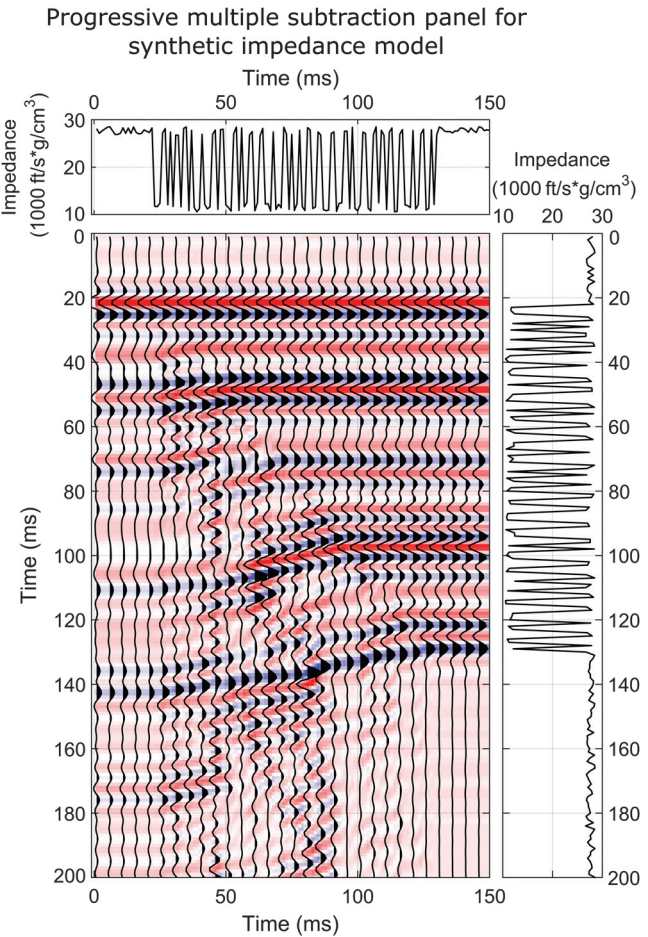


Figure 9. Progressive multiple subtraction panel for the impedance model shown in Figure 7a. Time-domain impedance logs are plotted for lithologic identification. The leftmost trace in the seismic display is the synthetic seismogram with all multiples, and the rightmost trace in the seismic display is the synthetic seismogram with primary-only reflections.

1985b). To illustrate the smoothing effects caused by coarse time sampling, the impedance log was converted to time with sampling rates of 0.5, 1, and 2 ms. Then, the time-domain impedance logs are converted back to depth using a time-depth table and overplotted on the original impedance log (Figure 5). The primary-only synthetic seismograms from the 0.5, 1, and 2 ms sampled impedance logs in Figure 5 are shown in Figure 6a along with a multiple synthetic plotted in black. The primary-only synthetics with the three different sample rates overlie one another in Figure 6a. The synthetic seismograms with multiples are sensitive to the sampling rate used in the depth-to-time conversion process. The finer sampling rate delays the reflections more and increases the correlation between the synthetic and seismic. The reflection delays can be quantitatively measured from the two-way transmitted wavefields reflected at the bottom of the coal-bed sequence (Figure 6c).

There are alternate methods for computing synthetic seismograms with multiples that do not require equal time sampling of

the impedance log (Ganley, 1981). These methods easily allow absorption models in the forward-modeling process. However, the multiple synthetic as shown in Figure 1 is an excellent match to the seismic, and additional attenuation does not appear to be needed for an interpretational match. Likewise, the time-domain forward-modeling method proposed by Waters (1987) is efficient and accurate with little numerical dispersion problems even for long multiple trains. Therefore, the Goupillaud model and the Waters (1987) algorithm are used to generate synthetic seismograms and transmitted wavefields within the paper.

PROGRESSIVE REMOVAL OF SF EFFECTS

Using equation 3 and the two-way transmitted wavefield in equation 7, a synthetic with multiples $R_M(z)$ can be expressed as a convolution with the primary reflection coefficients c_i and the nonstationary transmitted wavefield (Qi, 2013):

$$R_M(z) = \sum_{i=0}^M \hat{W}_i(z) c_i z^i. \quad (9)$$

If multiple reflections and transmission effects are not considered, the reflection response in a layered model is just the multiplication of two polynomials (the conventional convolution model):

$$P_M(z) = W(z) C_M(z), \quad (10)$$

$$C_M(z) = \sum_{i=0}^M c_i z^i. \quad (11)$$

Equation 9 is referred to as a time-varying convolution, and equation 10 is just a special case when the propagating wavelet is stationary (not evolving with time).

Equation 9 is a forward-modeling process, and now, an inverse-modeling process will be discussed with the goal of being able to correlate events on a multiple synthetic to a primary-only synthetic. Equation 9 is a time-varying convolution in which the transmitted wavelet varies for each time sample and the other time series is the primary reflectivity. Essentially, a time-varying deconvolution is developed so that upon completion, the multiple synthetic is converted into the primary-only synthetic. This model-based multiple removal process is done progressively such that from step 1 to step M , interbed multiples due to interface 1 to interface M are removed step by step. The output trace at step k for a M -layer model has the notation $R_{M,k}(z)$, and it is composed of primary-only reflection coefficients before time k and multiples plus primaries after time k :

$$R_{M,k}(z) = C_k(z) + \sum_{i=k+1}^M \frac{\hat{W}_i(z) c_i z^i}{\hat{W}_k(z)}, \quad (12)$$

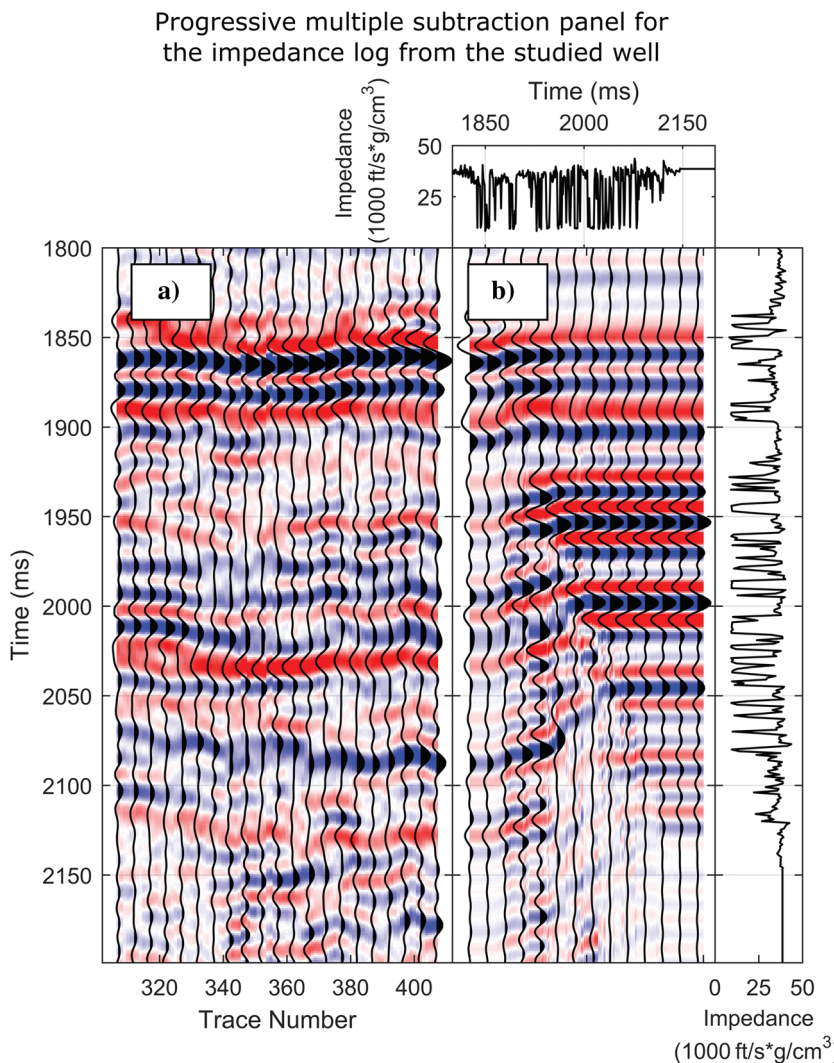


Figure 10. (a) Near-stack seismic data are plotted by the (b) progressive multiple subtraction panel for correlating seismic data to the primary-only synthetic seismogram. Impedance logs are shown at top and right side of (b). The leftmost trace in (b) is the synthetic seismogram with all internal multiple reflections.

$$C_k(z) = \sum_{i=0}^k c_i z^i. \quad (13)$$

The term k is in the range of zero to M . The function $R_{M,0}(z)$ is equivalent to $R_M(z)$ in equations 1, 3, and 9, the impulse reflection response with all possible raypaths. Similarly, $R_{M,M}(z)$ is equivalent to $P_M(z)$ in equation 10, the reflection-coefficient series. Because $\hat{W}_k(z)$ represents the two-way transmitted wavefield from interface 0 to interface k then back to interface 0, the $C_k(z)$ term in equation 12 represents the seismogram without the SF effects related to layers above interface k . It should be noted that any interbed multiples due to deeper interfaces, e.g., the raypath reflected from interface $k+1$ and bouncing among interfaces shallower than k have not been removed at step k .

To make a correlation with the primary-only synthetic seismogram, the synthetic seismogram with all interbed multiples is deconvolved gradually using equation 12. The deconvolved seismograms, when visualized sequentially, illustrate the evolution of the synthetic seismogram with all orders of multiples to the synthetic seismogram with primary reflections only. The following steps summarize the workflow:

- 1) Analyze and extract the proper sampling rate and source wavelet to match the multiple synthetic seismogram to the seismic trace at the well location.
- 2) Calculate the two-way transmitted wavefields at each time sample using equations 5–7.
- 3) Calculate the inverse filters for each two-way transmitted wavefield derived from step 2.
- 4) For computing the output trace at sample k , convolve the k th inverse filter calculated at step 3 with the nonstationary convolution trace $\sum_{i=k+1}^M \hat{W}_i(z) c_i z^i$ per equation 12, and pad the first $k-1$ samples with reflection coefficient series c .
- 5) Convolve the output trace from step 4 with the estimated source wavelet from step 1.
- 6) Repeat steps 4 and 5 until all samples have been deconvolved. Arrange the output traces sequentially.

RESULT

First, we tested the progressive multiple subtraction method on a synthetic model that contains only two lithologies: sand and coal. The sand has a velocity of 12,000 ft/s (3657 m/s) and density of 2.3 g/cm³, whereas the coal has a velocity of 7700 ft/s (2346 m/s) and density of 1.5 g/cm³. The impedance contrast leads to a reflection coefficient as high as –0.41 for the normal-incident wave traveling from sand to coal. The thickness of the 30 coal and shale beds randomly varied from 1 to 3 ms in terms of the two-way traveltimes (Figure 7a). Figure 7b illustrates the first 30 ms of the two-way transmitted wavefields that are aligned based on their corresponding basic primary arrival time. Figure 7a and 7b shares the same horizontal two-way traveltime axis, so the two-way transmitted wavefield at a certain time can be correlated with the impedance log. Prior to entering the coal-bed sequence, the peaks of the two-way transmitted wavefields in Figure 7b are not delayed relative to the basic primary reflections. However, upon traveling into coal beds, not only the peaks of the two-way transmitted wavefields suffer from increasing delays, but also the wavelet (the front end of the wavefield) becomes broader as well. Figure 7c shows the amplitude

spectra of the two-way transmitted wavefields for locations at 40, 80, and 120 ms. SF acts like a high-cut filter leaving only the low frequency after traversing the coal beds, which implies that the signal-to-noise ratio (S/N) below the coal beds could be enhanced by high-cut filters. To illustrate the impact of SF on the seismic well tie, we compared in Figure 8 the synthetic seismogram with primary plus multiple reflections using the Waters algorithm $R_M(z)$ to the synthetic seismogram with primary-only reflection coefficients. Both seismograms are convolved with the same Ormsby filter (0–10–150–200 Hz). The two synthetic seismograms are easily correlated to each other for the first 60 ms but notice the difference in the amplitude. After 60 ms, the two synthetics diverge in character. For the first 60 ms, a simple stretch on $C_M(z)$ creates a good phase correlation with $R_M(z)$, but as noted, the amplitude correlation is incorrect and would lead to erroneous estimates of elastic properties during an inversion. As more coal beds are encountered, as shown in Figure 7b, significant stretching decreases the fidelity of the interpretation.

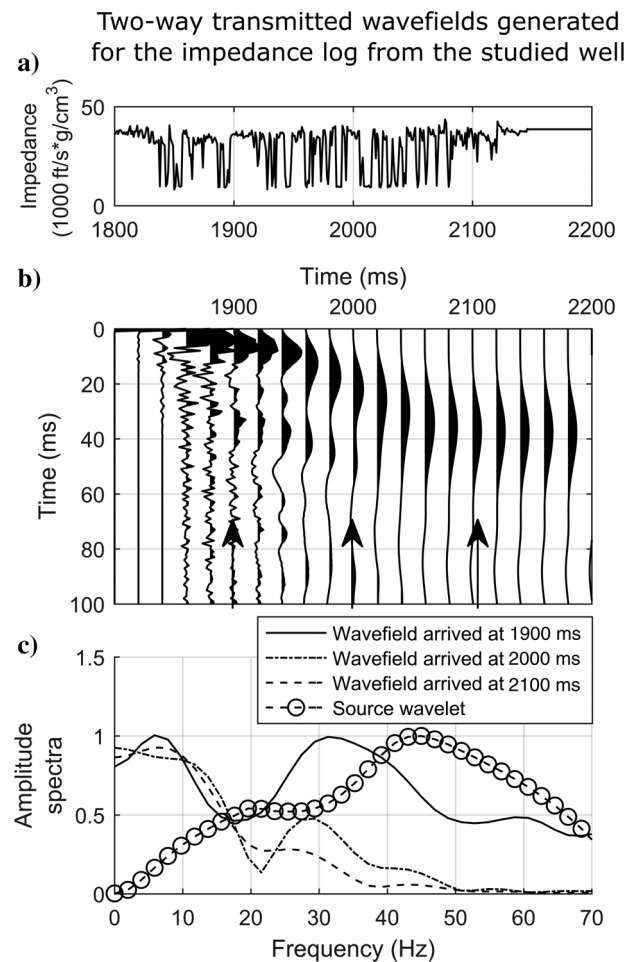


Figure 11. (a) Time-domain impedance log and (b) the corresponding two-way transmitted wavefields. (c) Amplitude spectra of two-way transmitted wavefields at the top, middle, and the bottom of the coal-bed sequence are plotted along with the spectrum of the extracted source wavelet.

It is instructive to show the path that reveals the evolution of the primary-only synthetic seismogram $C_M(z)$ in Figure 8b to the primary plus internal multiple synthetic seismogram $R_M(z)$ in Figure 8a. Such an evolution is illustrated in Figure 9 using the progressive multiple subtraction method (equation 12). The top and the right panels are impedance logs with the same time scales as the horizontal and the vertical axes of the central panel in Figure 9. From left to right of the main panel in Figure 9, the multiples are removed progressively starting from the top, and this slow progression allows one to correlate $R_M(z)$ to $C_M(z)$ with reasonable confidence. At less than 140 ms in $R_M(z)$, there are no obvious correlation trends connecting to $C_M(z)$, which implies that all reflection events of less than 140 ms in the original seismogram are noise (not related to the primary reflections).

The synthetic example illustrates the well-tie effectiveness of the progressive multiple subtraction method with severe SF. One of the first steps to successfully interpret the lithology using progressive multiple subtraction is to correlate the synthetic with multiples $R_M(z)$ to the poststack seismic data. With careful source wavelet extraction and log editing, we achieved good synthetic matches

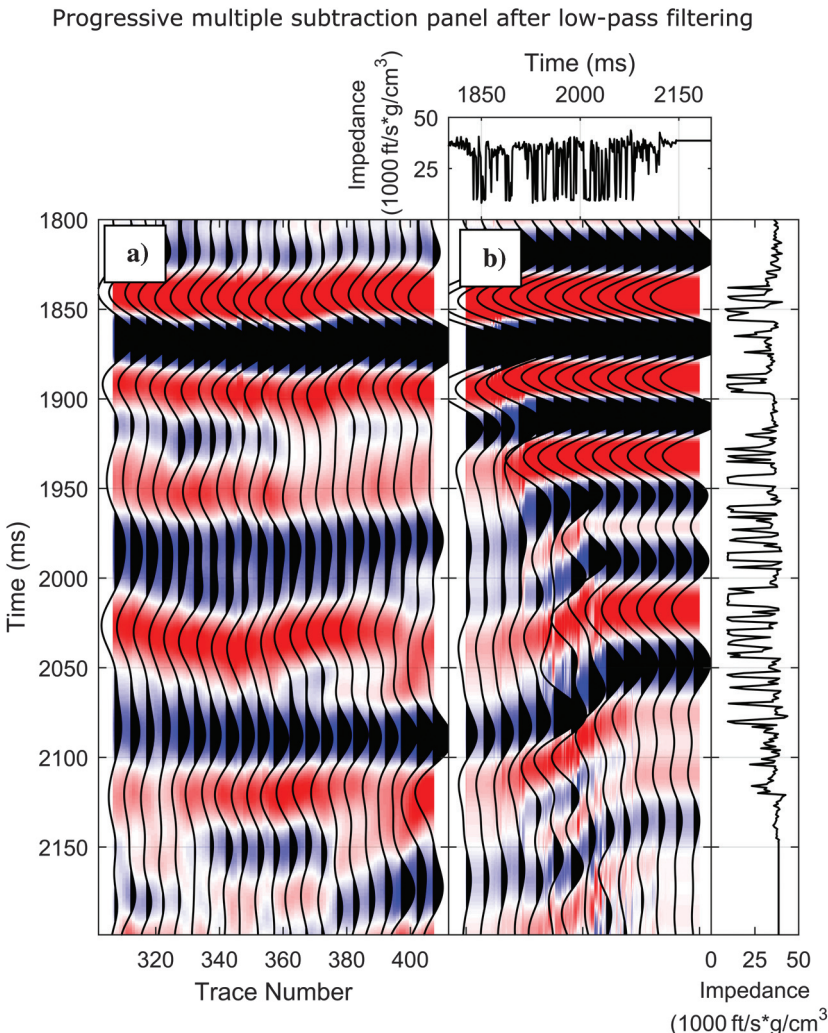


Figure 12. (a) Near-offset stack and (b) progressive multiple subtraction panel with 0–40 Hz passband.

in areas with more than 30 coal beds (Figure 1). We applied progressive multiple subtraction to tie seismic reflection events to primary-only synthetic seismogram. At the well location on the near-offset stack (Figure 10a), the progressive multiple subtraction panel is inserted (Figure 10b) to facilitate the correlation of reflection events from the seismic data to the multiple synthetic and across the progressive multiple panel to the primary-only reflections and thus correlate to the lithologic interfaces in the impedance log.

However, as indicated in Figure 10b, not all trends from left to right are continuous because of the long-path multiple reflections. Unlike the synthetic example shown in Figure 9, the long-path multiples start to interfere with the generalized primary reflections earlier and impair the continuity of the correlation trends. To analyze the problem we compute two-way transmitted wavefields (Figure 11b), and their spectra are shown in Figure 11c. The impedance log in Figure 11a indicates the beds that were traversed by the two-way transmitted wavefields. Due to excessive thin beds and high impedance contrast introduced by Permian coal beds, a 40 ms reflection delay is observed at the bottom of the coal beds. Figure 11c

compares the amplitude spectra of the two-way transmitted wavefields at 1900, 2000, and 2100 ms and the amplitude spectrum of the seismic source wavelet used to construct the synthetic seismograms. The SF attenuation filters the two-way transmitted wavefields below the coal bed sequence to a 0–40 Hz bandwidth. Comparing the spectrum of the source wavelet against the spectrum of the wavefield arriving less than 2100 ms suggests that low-frequency enhancement is necessary for further acquisition and reprocessing.

Therefore, to achieve a better S/N at the bottom of the thick coal bed sequence, a high-cut filter that excludes the frequency bandwidth outside of the bandwidth of the corresponding two-way transmitted wavefield at the bottom of the coal bed sequence is applied to the near-offset seismic and the multiple subtraction panel shown in Figure 11a and 11b. The result is shown in Figure 12. Even though the seismic resolution is inevitably lost by the high-cut filtering, the structural interpretation below the bottom of the coal-bed sequence is increased, and we can estimate the thickness of the coal-bed sequence.

CONCLUSION

SF delays seismic reflections and attenuates propagating wavelets. In highly cyclically stratified sedimentation, SF impacts the interpretation through the well tie. To analyze such effects, we capitalized on the idea of generalized primary reflections and extended it with the two-way transmitted wavefields and the corresponding progressive multiple subtraction. With well logs, we can easily determine the arrival-time delay for any reflectors by computing the two-way transmitted wavefields and picking the peak arrivals. The modification of the time-depth table can be

done with the time-delay curve analyzed from two-way transmitted wavefields. However, a better solution is to correlate directly from the seismic to the primary-only synthetic seismogram using progressive multiple subtraction. This process progressively removes the transmission effects of SF to derive the correlation trends connecting the seismic with all primary and multiple reflections to the synthetic seismogram with only primary reflections. The long-path multiple reflections do not have continuous correlation trends, and sometimes the interference of these multiples impairs the ability to correlate the corresponding seismic event to the lithologic boundaries that are defined by the impedance log. A high-cut filter designed per the spectra of the two-way transmitted wavefields improves the S/N and could be applied on the near-offset stack to define bed boundaries.

ACKNOWLEDGMENTS

The authors appreciate the financial support from Geokinetics and Beach Energy. Seismic data and well-log data are provided by Beach Energy. We also appreciate the help from L. Bell, F. Nicholson, and other colleagues from Geokinetics and Beach Energy for their insightful suggestions and instructions.

REFERENCES

- Banik, N. C., I. Lerche, and R. T. Shuey, 1985a, Stratigraphic filtering, Part 1 — Derivation of the O'Doherty-Anstey formula: *Geophysics*, **50**, 2768–2774, doi: [10.1190/1.1441897](https://doi.org/10.1190/1.1441897).
- Banik, N. C., I. Lerche, and R. T. Shuey, 1985b, Stratigraphic filtering, Part 2 — Model spectra: *Geophysics*, **50**, 2775–2783, doi: [10.1190/1.1441898](https://doi.org/10.1190/1.1441898).
- Claerbout, J., 1968, Synthesis of a layered media from its acoustic transmission response: *Geophysics*, **33**, 264–269, doi: [10.1190/1.1439927](https://doi.org/10.1190/1.1439927).
- Ganley, D. C., 1981, A method for calculating synthetic seismograms which include the effects of absorption and dispersion: *Geophysics*, **46**, 1100–1107, doi: [10.1190/1.1441250](https://doi.org/10.1190/1.1441250).
- Goupillaud, P. L., 1961, An approach to inverse filtering of near-surface layer effects from seismic records: *Geophysics*, **26**, 754–760, doi: [10.1190/1.1438951](https://doi.org/10.1190/1.1438951).
- Hubral, P., S. Treitel, and P. R. Gutowski, 1980, A sum autoregressive formula for the reflection response: *Geophysics*, **45**, 1697–1705, doi: [10.1190/1.1441061](https://doi.org/10.1190/1.1441061).
- Kunetz, G., 1964, Generalisation des opérateurs d'antiresonance à un nombre quelconque de réflecteurs: *Geophysical Prospecting*, **12**, 283–289, doi: [10.1111/j.1365-2478.1964.tb01904.x](https://doi.org/10.1111/j.1365-2478.1964.tb01904.x).
- Lupinacci, W. M., A. P. de Franco, S. A. M. Oliveira, and F. S. de Moraes, 2017, A combined time-frequency filtering strategy for *Q*-factor compensation of poststack seismic data: *Geophysics*, **82**, no. 1, V1–V6, doi: [10.1190/geo2015-0470.1](https://doi.org/10.1190/geo2015-0470.1).
- Margrave, G. F., 2015, Using well logs to estimate the effect of fine layering on *Q* estimation: 85th Annual International Meeting, SEG, Expanded Abstracts, 3181–3185.
- Margrave, G. F., M. P. Lamoureux, and D. C. Henley, 2011, Gabor deconvolution: Estimating reflectivity by nonstationary deconvolution of seismic data: *Geophysics*, **76**, no. 3, W15–W30, doi: [10.1190/1.3560167](https://doi.org/10.1190/1.3560167).
- Mathieu, J. D., 2013, High-frequency recovery of surface seismic data from autoregressive spectral extrapolation and *Q*-compensation: 83rd Annual International Meeting, SEG, Expanded Abstracts, 2448–2452.
- O'Doherty, R. F., and N. A. Anstey, 1971, Reflections on amplitudes: *Geophysical Prospecting*, **19**, 430–458, doi: [10.1111/j.1365-2478.1971.tb00610.x](https://doi.org/10.1111/j.1365-2478.1971.tb00610.x).
- Qi, C., 2013, Seismic characterization of coal interbed multiples in Cooper Basin, Australia: M.S. thesis, University of Houston.
- Qi, C., and F. J. Hilterman, 2014, Quantification of signal and noise in two-way transmitted wavefields to improve well ties in Cooper Basin, Australia: *Interpretation*, **2**, SD19–SD31, doi: [10.1190/INT-2013-0129.1](https://doi.org/10.1190/INT-2013-0129.1).
- Qi, C., and F. J. Hilterman, 2015, Removal of coal bed multiples: 85th Annual International Meeting, SEG, Expanded Abstracts, 4470–4474.
- Robinson, E. A., 1967, Multichannel time series analysis with digital computer programs: Holden Day Inc.
- Robinson, E. A., 1968, Basic equations for synthetic seismograms using the z-transform approach: *Geophysics*, **33**, 521–523, doi: [10.1190/1.1439949](https://doi.org/10.1190/1.1439949).
- Stovas, A., Y. Roganov, K. Duffaut, and A. J. Carter, 2007, Low-frequency layer-induced anisotropy: *Geophysics*, **78**, no. 5, WC3–WC14, doi: [10.1190/geo2012-0301.1](https://doi.org/10.1190/geo2012-0301.1).
- Treitel, S., and E. A. Robinson, 1966, Seismic wave propagation in layered media in terms of communication theory: *Geophysics*, **31**, 17–32, doi: [10.1190/1.1439729](https://doi.org/10.1190/1.1439729).
- Waters, K. H., 1987, *Reflection seismology*: John Wiley and Sons Inc.